Supplement of Atmos. Chem. Phys., 25, 9497–9518, 2025
https://doi.org/10.5194/acp-25-9497-2025-supplement

Atmospheric Chemistry and Physics
Open Access

Supplement of

Changes in the impacts of ship emissions on $PM_{2.5}$ and its components in China under the staged fuel oil policies

Guangyuan Yu et al.

Correspondence to: Yan Zhang (yan_zhang@fudan.edu.cn) and Cheng Huang (huangc@saes.sh.cn)

Text S1. Technical information on the CMAQ code revision for V and Ni.

For the revision of modules for simulate V and Ni in the CMAQ, we modified desid_vars.F to add V and Ni emission information. Then, we modified AERO_DATA.F, CMAQ_Control_DESID_cb6r5_ae7_aq.nml, and AE_cb6r5_ae7_aq.nml files to add V and Ni in the CMAQ output. V and Ni are regarded as inert traces which undergo the same diffusion, advection, and deposition as PM.

Text S2. Technical details on the setup of the ship emission model.

In this study, ship emissions were calculated based on a bottom-up activity-based method. The main engine (ME) load factor, LF_m, was calculated as follows:

$$LF_m = (S_a/S_{max})^3 \quad \text{(S1)}$$

where S_a is the actual speed when ship is cruising and S_{max} is the maximum speed for the ship.

Main engine emissions, E_m (g), were calculated as follows:

$$E_m = P_m \times LF_m \times LLAM \times FCF \times T_m \times EF_m \quad \text{(S2)}$$

where P_m is the installed power of ME (kW), $LLAM$ is the low load adjustment multiplier for the main engine (Table S14), FCF is the fuel correction factor, T_m is the operation time of the main engine (h), and EF_m is the main engine emissions factor (g/kWh).

Auxiliary engine (AE) emissions, E_a (g), were calculated as follows:

$$E_a = P_a \times LF_a \times T_a \times EF_a \quad \text{(S3)}$$

where P_a is the installed power of the auxiliary engine (kW), LF_a is auxiliary engine load factors, T_a is operation time of the auxiliary engine (h), and EF_a is the auxiliary engine emissions factor (g/kWh).

The total ship emissions, E (g), was calculated as follows:

$$E = E_m + E_a \quad \text{(S4).}$$

Auxiliary boiler emissions were not considered in this study because limited auxiliary boiler information exists in the Lloyd's register and Chinese Classification Society (CCS) database. The engine fuel correction factors (FCFs) were set to 1 in this study because we set different emission factors by ship type (marine or inland ship) and policy stages as described in Sect. 2.2.1.

For ships available in Lloyd's register and CCS database, the following data were derived from these

databases including ship name, ship type, date of construction, flag name, revolutions per minute (RPM) of the main engine, speed, maximum design power of the main engine, maximum design power of the auxiliary engines, and gross tonnage. Information of some domestic ships is available in CCS database, but for those ships unavailable in the database, default values of the main engine power averages were uniformly applied to different ship types: oil tankers (2400 kW), container cargo ships (5000 kW), non-container cargo ships (3800 kW), passenger ships (2300 kW) and other types of ships (2300 kW).

Text S3. Details on the model performance.

The model performance of the meteorological elements is shown in Table S9. the model can outstandingly reproduce the 2-m temperature in each city during the 11 simulated months from 2017 to 2021. Except for Qinzhou (r = 0.88), the r values of the other cities were all above 0.9, and over 0.95 for most cities. The performance for relative humidity was slightly inferior to that of temperature, with correlations ranging from 0.7 to 0.8 in most cities. Except for Dalian (NMB = 2.4%), all other cities show negative biases, which was caused by the underestimation of nighttime radiation cooling. For the 10-m wind speed, overestimation was found in most cities especially megacities such as Shanghai (NMB = 95.5%) and Shenzhen (NMB = 72.2%). The WRF model with a resolution of 9 km can generally reproduce the average wind direction at a station level which is significantly affected by local topography.

The model performance of the CMAQ model is shown in Table S10. Large biases of over ±50% of the concentration levels of SO_2 and NO_2 were found in three megacities including Shanghai, Shenzhen, and Beijing with positive biases, and in Qinzhou with negative biases. These biases were mainly caused by the uncertainties in the local emissions of the MEIC inventory. In general, the performance for the daily maximum 8-h average (MDA8) O_3 concentrations in the coastal cities showed the patterns of underestimation in Zhejiang province and to its north and overestimation in Fujian province and to its south, corresponding to the biases of NO_2 concentrations. The negative biases of the $PM_{2.5}$ concentrations were found in most port cities that we concerned, which was discussed in Sect. 3.2. The negative biases were larger in spring, which was likely due to insufficient consideration of heterogeneous reactions like reactions on the surface of mineral dust in the CMAQ model.

For the uncertainties of V and Ni concentrations, in Shanghai, the model tended to overestimate the concentrations of the two metals in winter, such as overestimating the concentrations of V and Ni in

January 2017 by 41% and 30%, respectively (Table S12). The pattern in July 2021 was underestimating both V and Ni concentrations by 38%. These results can be brought by uncertainties in the simulation of diffusion conditions. The CMAQ model was fed by monthly ship emissions, and the high-frequency ship traffic data was smoothed, resulting the relatively weak temporal correlation between observational data and simulation results with hourly resolution. The uncertainties in meteorology can also affect the simulation of the transport process of ship emissions to urban areas.

Besides, to evaluate the updated V and Ni emission inventories, we reviewed recently published studies, and compared the changes in the average ambient V and Ni concentrations in several coastal cities in the model domain since the DECA 1.0 period to the simulation results as follows:

In Qingdao, a port city in northern China, the observed mean concentrations of PM_1-bound V (Ni) during the periods with small impacts of long-range transport by northwesterly wind were 4.01 (3.03) ng m^{-3} during the DECA 1.0, 1.50 (2.13) ng m^{-3} during the DECA 2.0, and 0.84 (3.55) ng m^{-3} during the IMO 2020 Regulation (Du et al., 2024). The simulated average $PM_{2.5}$-bound V (Ni) concentrations in Qingdao were 5.9 (4.0) ng m^{-3} in 2017 and 1.6 (3.1) ng m^{-3} in 2021 in this study. The concentration levels and the reductions rate of V concentrations from the DECA 1.0 to the IMO 2020 Regulation based on observation and simulation were both comparable. However, the simulated V concentration during the DECA 2.0 (6.9 ng m^{-3}) was significantly higher compared to the observational result (1.50 ng m^{-3}) . One reason was that the observation was conducted in January and December when continental flows dominated marine flows, whereas the simulation was conducted in April with peak V concentrations. Another reason was that the ships navigating on the northern Yellow Sea generally combusted low sulfur fuel oil (LSFO) whether inside or outside the CECA during the DECA 2.0, which was different from the case regarding the Yangtze River Delta. The observed Ni concentrations fluatuated, which was likely due to the impact of other local sources.

In Jiaxing, a port city located next to Shanghai, the observed annual mean concentrations of $PM_{2.5}$-bound V (Ni) were 5.52 (4.68) ng m^{-3} in 2017, 4.29 (4.44) ng m^{-3} in 2019, and 1.34 (4.18) ng m^{-3} in 2021 (Zhang et al., 2024a). The simulated annual mean concentrations of V (Ni) were 8.3 (3.9) ng m^{-3} in 2017, and 1.2 (2.2) ng m^{-3} in 2021. The simulated monthly mean concentrations of V and Ni in April 2019 were 5.4 and 3.2 ng m^{-3}, respectively. Although the model overestimated the V concentration in 2017 and underestimated the Ni concentration in 2021, all the biases were within the range of ±50%.

In Xiamen, a port city in southeastern China, the observed annual mean concentrations of $PM_{2.5}$-bound

V (Ni) were 7.35 (3.22) ng m^{-3} in 2017–2018 and 1.60 (1.87) ng m^{-3} in 2022 (Li et al., 2025). The simulated annual mean V (Ni) concentrations were 9.0 (3.7) ng m^{-3} in 2017 and 1.2 (2.3) ng m^{-3} in 2021. The simulation results matched up with the observational results.

In Guangzhou, a large port city in southern China, the mean concentrations of $PM_{2.5}$-bound V and Ni from October 2019 to January 2020 were 1.1 ng m^{-3} and 3.1 ng m^{-3}, respectively (Zhang et al., 2024c). The closest simulation was conducted in April 2020, and the simulated monthly mean concentrations of V and Ni were 1.3 ng m^{-3} and 2.6 ng m^{-3}, respectively. The simulated concentrations were very close to the observed concentrations despite the fact that there was a gap between the studied periods.

Seoul, the capital of South Korea, can be impacted by ship emissions in the Yellow Sea. The observed annual mean concentrations of $PM_{2.5}$-bound V (Ni) in Seoul were 4.6 (1.7) ng m^{-3} in 2017 and 0.4 (0.5) ng m^{-3} in 2021 (Yeo et al., 2024). In comparison, the simulated concentrations were relatively lower in 2017 (V: 2.3 ng m^{-3}; Ni: 1.5 ng m^{-3}) and higher in 2021 (V: 0.6 ng m^{-3}; Ni: 1.1 ng m^{-3}), and thus the decrease rates were smaller, which was due to the uncertainties in the calculation of ship emissions in South Korea.

Overall, after updating the V and Ni emissions from shipping, the model could generally reproduce the decreasing trends of ambient V and Ni concentrations in China's coastal areas since 2017. More observational data in different areas are needed to better constrain the V and Ni emissions in local areas especially during the DECA 2.0 in the future.

Text S4. Overall changes in the impacts of ship emissions on air pollutants by annual average from 2017 to 2021.

The annual average represented by four months in 2017 and 2021 were used to show the overall changes due to the policy shift from the DECA 1.0 to the IMO Regulation.

Regarding the SO_2 concentrations from shipping, the P_{99} value in the model domain decreased from 2.6 μg m^{-3} in 2017 to 0.8 μg m^{-3} in 2021, with a reduction rate of 68.7% (Fig. S13). With a remarkable decrease in fuel sulfur content (FSC) globally, the SO_2 concentrations from shipping were reduced in all simulated areas. The largest reduction was observed in the lower reaches of the Yangtze River reaching 5.2 μg m^{-3} due to the fuel type shift to the ultra-low sulfur fuel oil (ULSFO).

Regarding the NO_2 concentrations from shipping, the P_{99} value increased from 8.1 μg m^{-3} in 2017 to 12.6 μg m^{-3} in 2021, with a increase rate of 54.6% (Fig. S14). The NO_2 concentrations increased in most areas from 2017 to 2021, and the increase was larger near the major ports with the maximum of 15.4 μg m^{-3}.

Regarding the shipping-related $PM_{2.5}$ concentrations, the P_{99} value was 2.5 μg m^{-3} in 2017 and decreased to 1.4 μg m^{-3} in 2021, with a reduction rate of 43.2% (Fig. S6a−c). In 2017, the areas with concentration over 1 μg m^{-3} covered most of the Yellow and Bohai Seas and extended to the Middle Yangtze River (~1000 km away from the coast). However, the areas with concentration over 1 μg m^{-3} shrunk to the coast and the central Yangtze River Basin in 2021. The areas with shipping-related $PM_{2.5}$ of over 0.1 μg m^{-3} occupied most of the model domain both in 2017 and 2021, which was markedly different from the patterns of SO_2 and NO_2 from shipping. This result is caused by sustained aging processes during the transport of ship-emitted pollutants as well as the longer lifetime of PM compared to SO_2 and NO_2 (Seinfeld and Pandis, 2016). The decrease in the concentrations of shipping-related $PM_{2.5}$ showed the largest value of 1.9 μg m^{-3} over Zhoushan Islands, while the slight increase within 0.5 μg m^{-3} was sporadically distributed over land areas.

Regarding the contributions of ship emissions to the $PM_{2.5}$ concentrations, in 2017, larger values of over 10% distributed along the main routes from the southern Yellow Sea to the northern South China Sea, with the maximum of 21.2% (Fig. 6d−f). The distance between the land areas with the contributions of over 4% and the coast could be up to ~300 km. The contributions were not less than 1% in the model domain except for northwestern China. In 2021, the areas with relative impact values exceeding 10% shrunk significantly, with the maximum of 16.9%. The largest decrease in the contributions was 11.0 percentage points. However, there were small positive changes scattering in China's inland areas. This result may be caused by the increase in nitrate formation related to shipping and the decrease in land-based anthropogenic emissions.

Regarding the V concentrations from shipping, the P_{99} value was reduced almost an order of magnitude (88.7%) from 11.4 ng m^{-3} in 2017 to 1.3 ng m^{-3} in 2021 (Fig. S9). The P_{99} value of the Ni concentrations from shipping was reduced by 31.5% from 3.6 ng m^{-3} in 2017 to 2.4 ng m^{-3} in 2021 (Fig. S10). In 2017, the areas with the V concentration from shipping exceeding 0.5 ng m^{-3} covered most parts of eastern China, and ship emissions overwhelmingly dominated the V concentrations in the marine and coastal areas as well as along the Yangtze River. Over land areas, the contributions of ship emissions to the Ni

concentrations were lower compared to V. In 2021, in the coastal areas, the contributions of land-based emissions to V were closed to or even higher than those of ship emissions. There was also an evident decrease in the contribution of ship emissions in remote marine areas because V from land-based emissions including anthropogenic sources and mineral dust can be transported by the high-altitude westerly wind. It is noted that the reduction in the Ni concentration share from 2017 to 2021 was small in the model domain, and the Ni concentration share overtook the V concentration share in 2021.

Regarding the shipping-related SO_4^{2-} concentrations, the P_{99} value was reduced by 72.1% from 1.0 μg m^{-3} in 2017 to 0.3 μg m^{-3} in 2021 (Fig. S15). In 2021, there were unexpected negative values over land areas, which was likely due to the depletion of oxidants to generate nitric acid (HNO_3) in areas characterized by high-NO_x conditions. Regarding the shipping-related NO_3^- concentrations, the P_{99} value increased by 24.3% from 0.7 μg m^{-3} in 2017 to 0.9 μg m^{-3} in 2021. Regarding the shipping-related NH_4^+ concentrations, the P_{99} value decreased by 20.6% from 0.4 μg m^{-3} in 2017 to 0.3 μg m^{-3} in 2021 because the overall reduction rate of the sulfate concentrations was higher than that of the nitrate concentrations.

Regarding the POA concentrations from shipping, the P_{99} value decreased by 65.7% from 0.2 μg m^{-3} in 2017 to 0.1 μg m^{-3} in 2021 (Fig. S16). The contributions of ship emissions to the POA concentrations were generally higher compared to the $PM_{2.5}$ concentrations, up to 41.9% in 2017 and 29.4% in 2021.

The potential impacts of ship emissions on the SOA and SO_4^{2-} concentrations shared similar spatial patterns in 2017, and no negative value was found in the entire model domain (Fig. S17a). However, the spatial pattern changed significantly in 2021. The marine and coastal areas displayed positive values with the maximum of 0.3 μg m^{-3}, whereas negative values were obtained inland with the minimum of -0.3 μg m^{-3} (Fig. S17b).

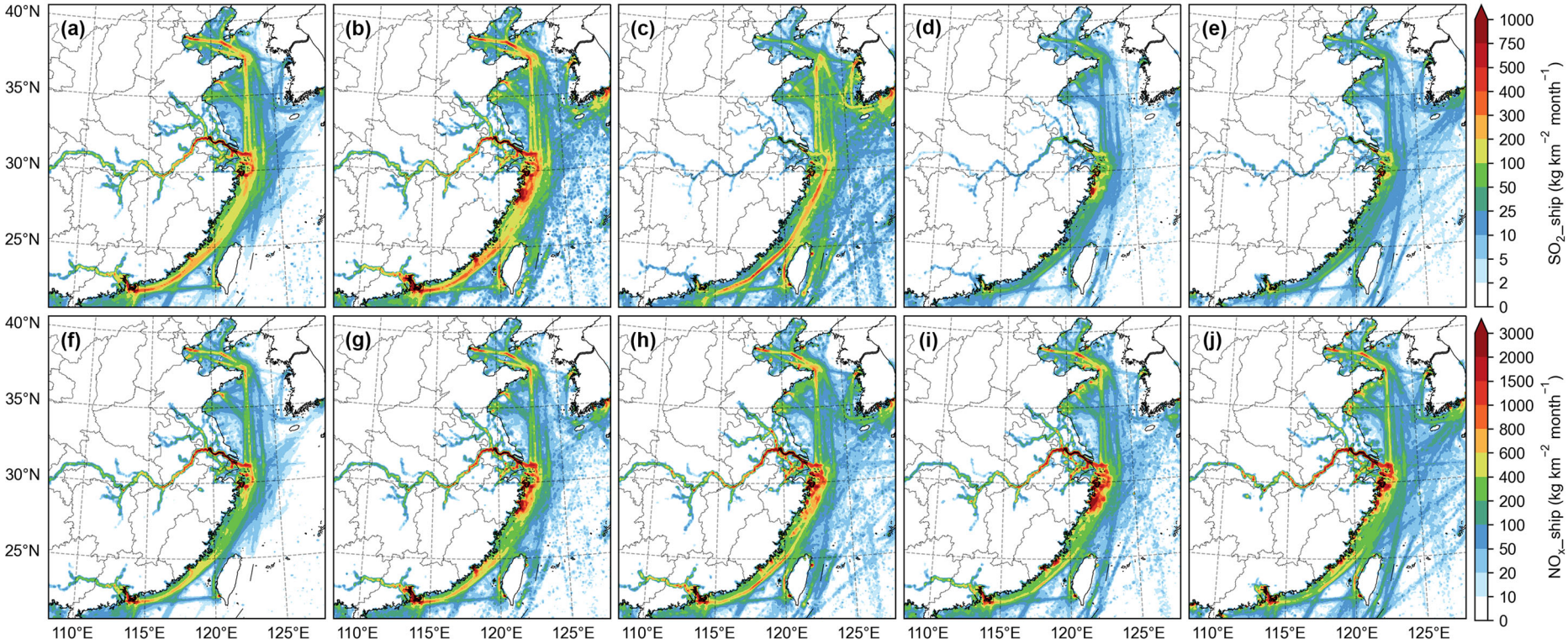

Figure S1. Spatial distributions of (a–e) the SO_2 emissions from shipping (SO_2_ship) and (f–j) the NO_x emissions from shipping (NO_x_ship) in Domain 2 of the CMAQ model in April from 2017 to 2021 in the chronological order from left to right.

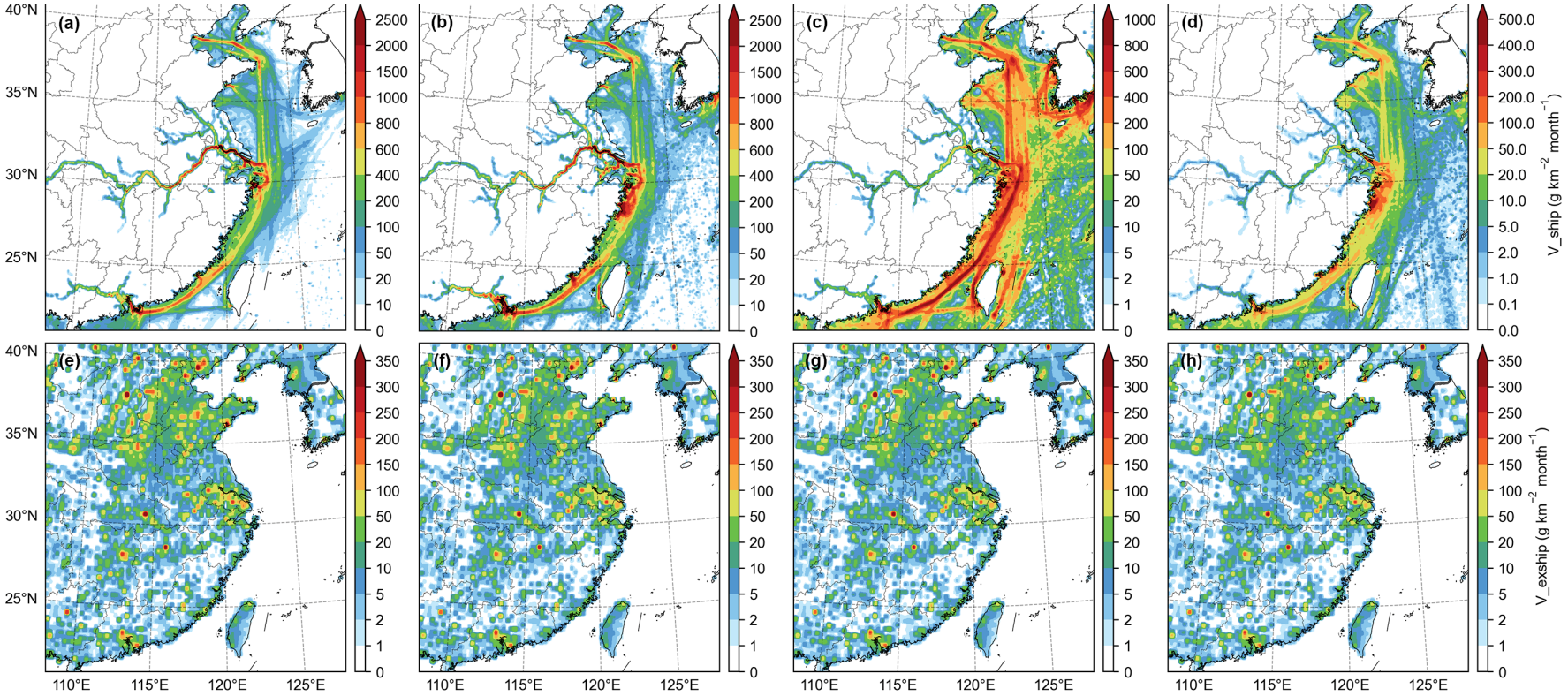

Figure S2. Spatial distributions of V emissions from shipping (V_ship) in (a) April 2017, (b) April 2018, (c) April 2019, and (d) April 2020; and spatial distribution of V emissions from anthropogenic sources excluding shipping (V_exship) in (e) April 2017, (f) April 2018, (g) April 2019, and (h) April 2020.

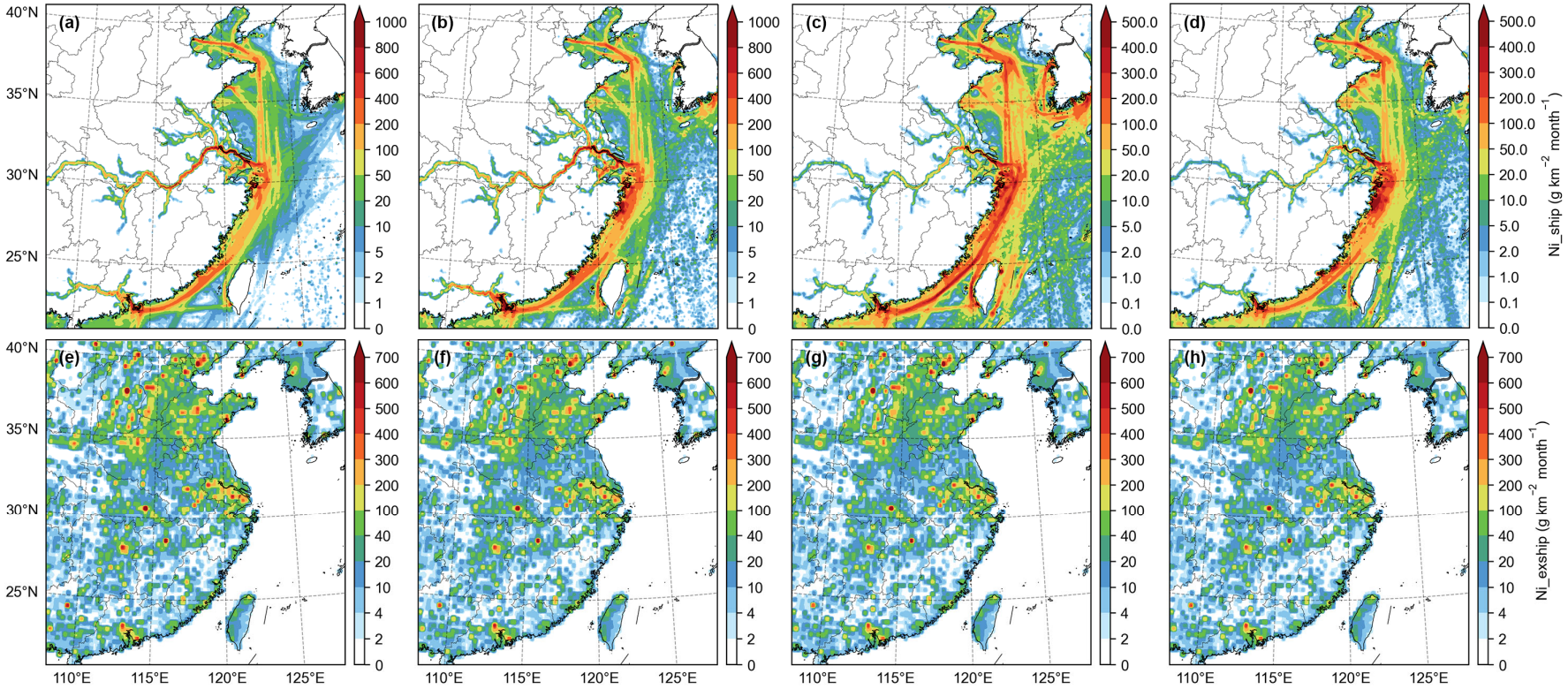

Figure S3. Spatial distributions of Ni emissions from shipping (Ni_ship) in (a) April 2017, (b) April 2018, (c) April 2019, and (d) April 2020; and spatial distribution of Ni emissions from anthropogenic sources excluding shipping (Ni_exship) in (e) April 2017, (f) April 2018, (g) April 2019, and (h) April 2020.

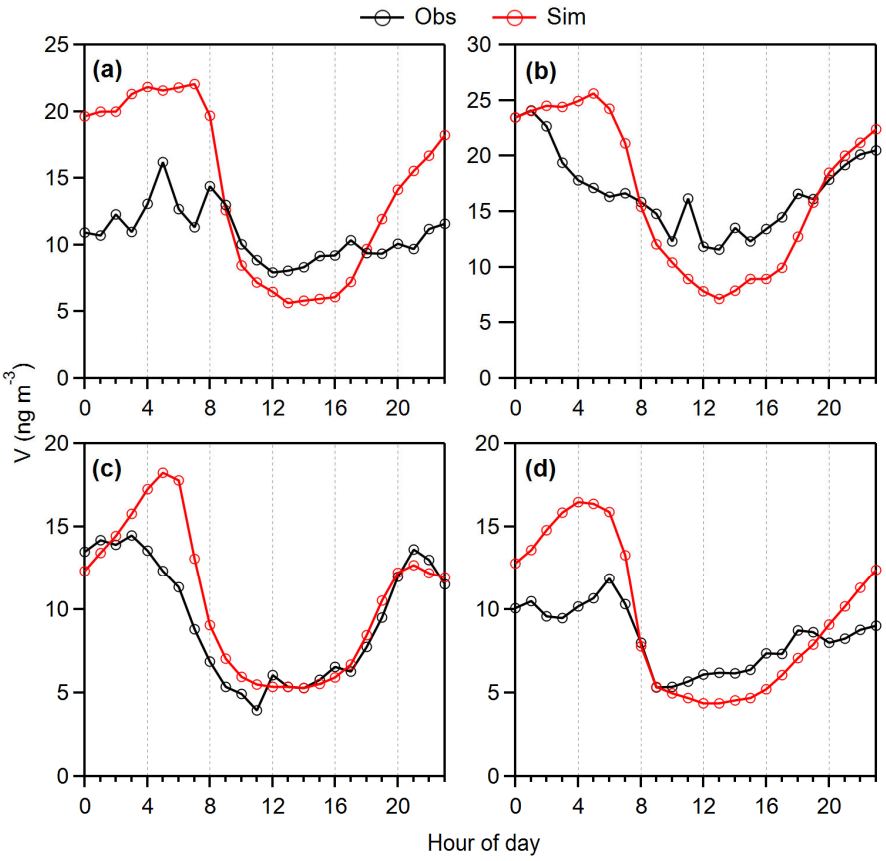

Figure S4. Comparison of observed (Obs) and simulated (Sim) diurnal variations of the V concentrations at the Pudong site of Shanghai in (a) January, (b) April, (c) July, and (d) October of 2017.

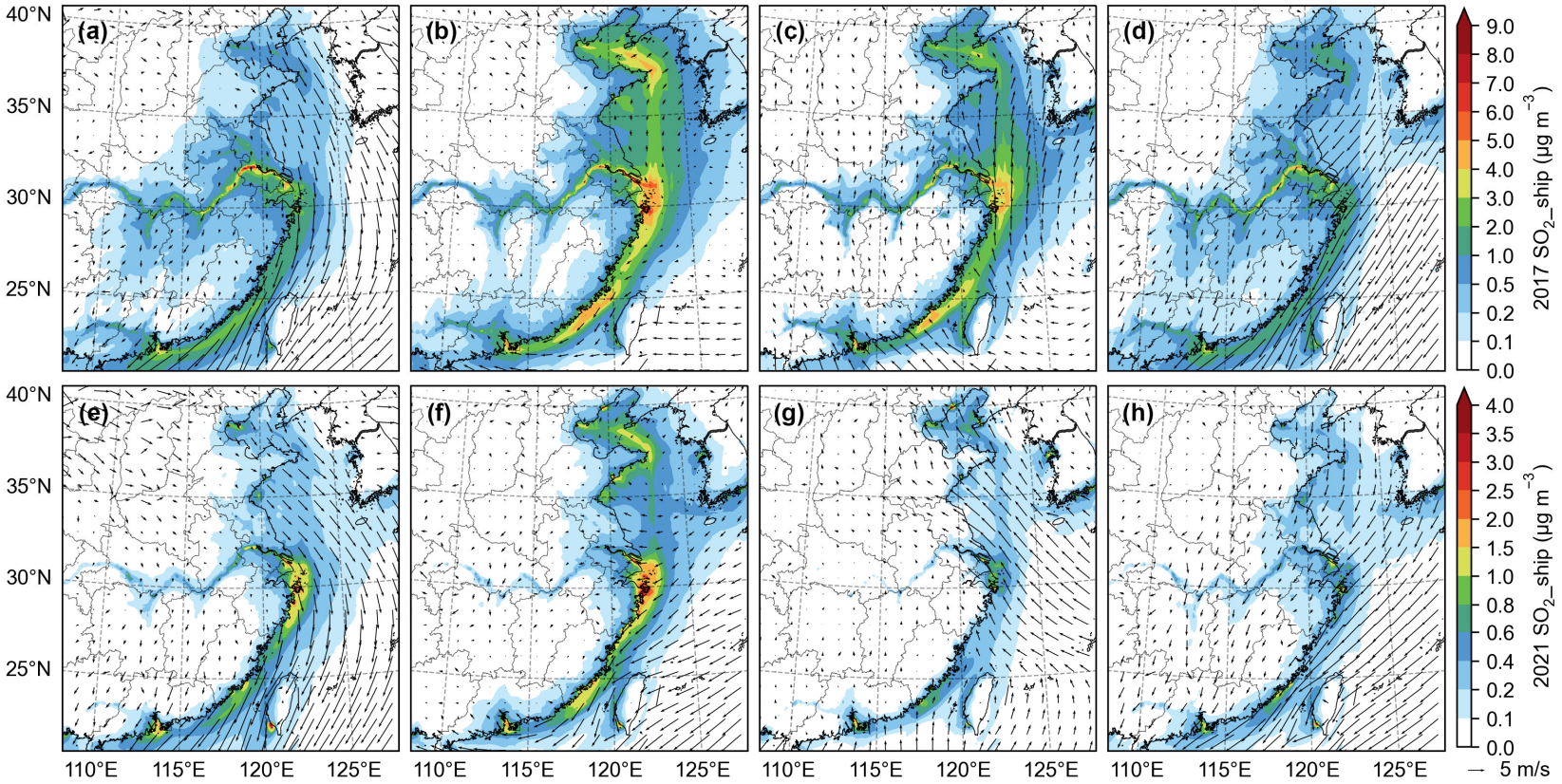

Figure S5. Seasonal variations of the impacts of ship emissions on the SO_2 concentrations (SO_2_ship) and simulated wind fields in (a) January 2017, (b) April 2017, (c) July 2017, (d) October 2017, (e) January 2021, (f) April 2021, (g) July 2021, and (h) October 2021.

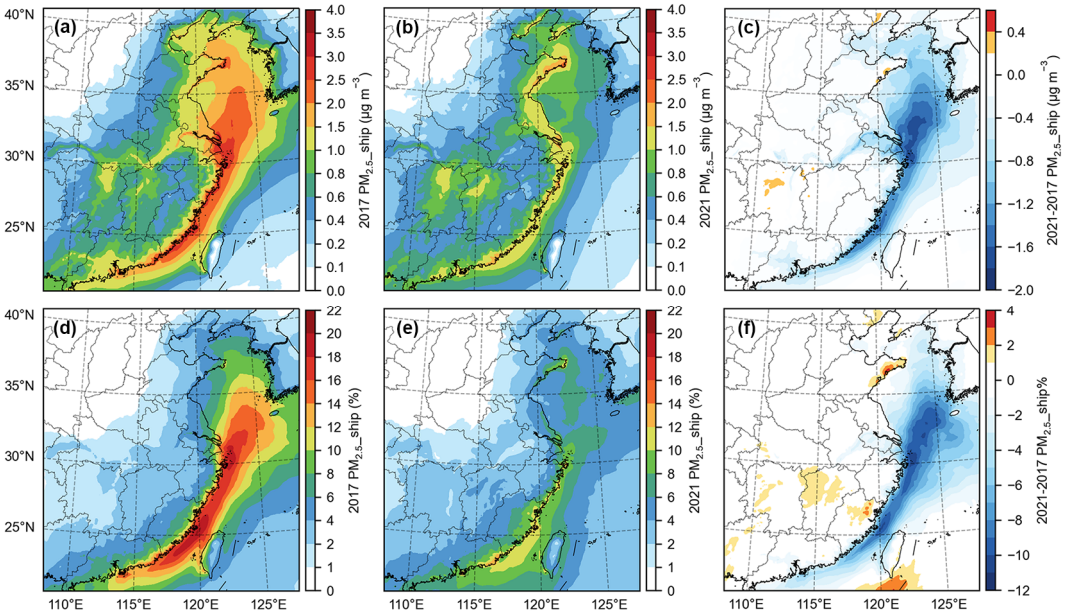

Figure S6. Potential impacts of ship emissions on $PM_{2.5}$ ($PM_{2.5}$_ship): for concentration (in μg m^{-3}) in (a) 2017 and (b) 2021, as well as (c) the absolute change from 2017 to 2021; and for contribution (in %) in (d) 2017 and (e) 2021, as well as (f) the change of percentage from 2017 to 2021 (in percentage point).

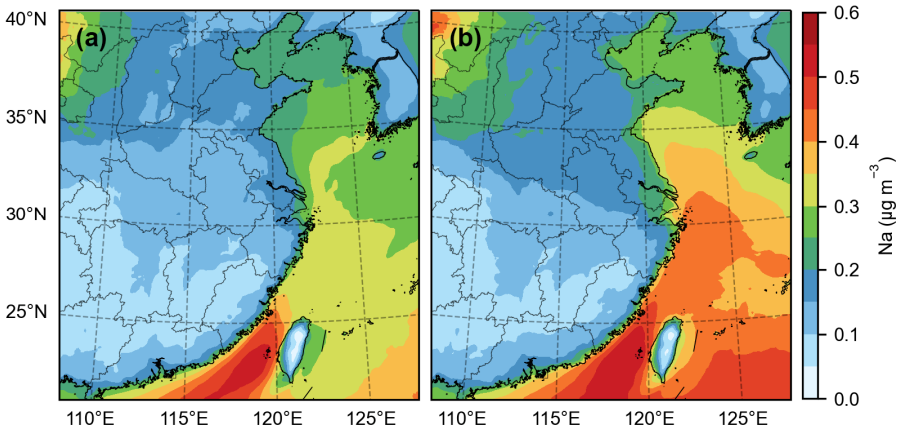

Figure S7. Spatial distributions of the sodium (Na) concentrations in $PM_{2.5}$ in (a) 2017 and (b) 2021.

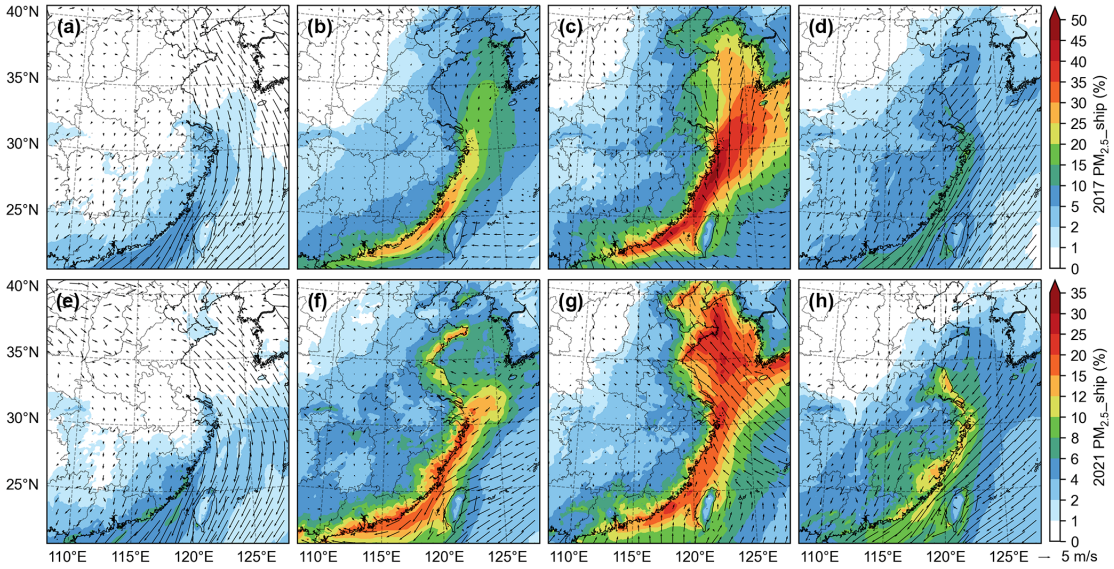

Figure S8. Seasonal patterns of the potential impacts of ship emissions on $PM_{2.5}$ ($PM_{2.5}$_ship) for contribution as well as the simulated monthly average wind fields in (a) January, (b) April, (c) July, and (d) October of 2017; and (e) January, (f) April, (g) July, and (h) October of 2021.

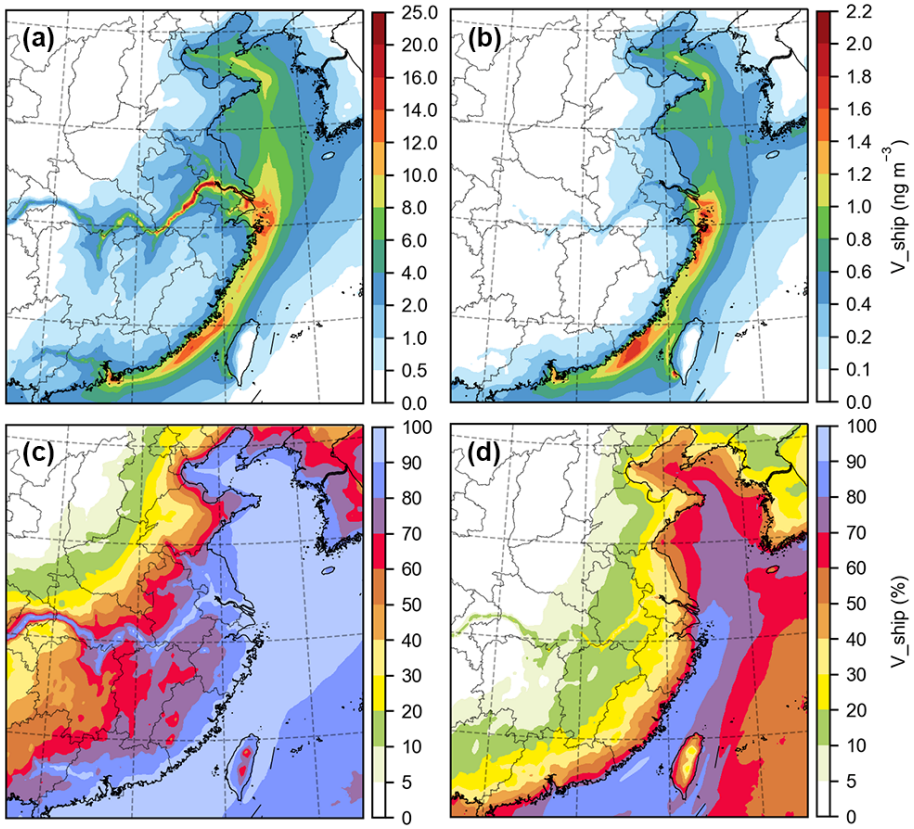

Figure S9. Impacts of ship emissions on V (V_ship): for concentration (in ng m^{-3}) in $PM_{2.5}$ in (a) 2017 and (b) 2021; and for contribution (in %) in (c) 2017 and (d) 2021.

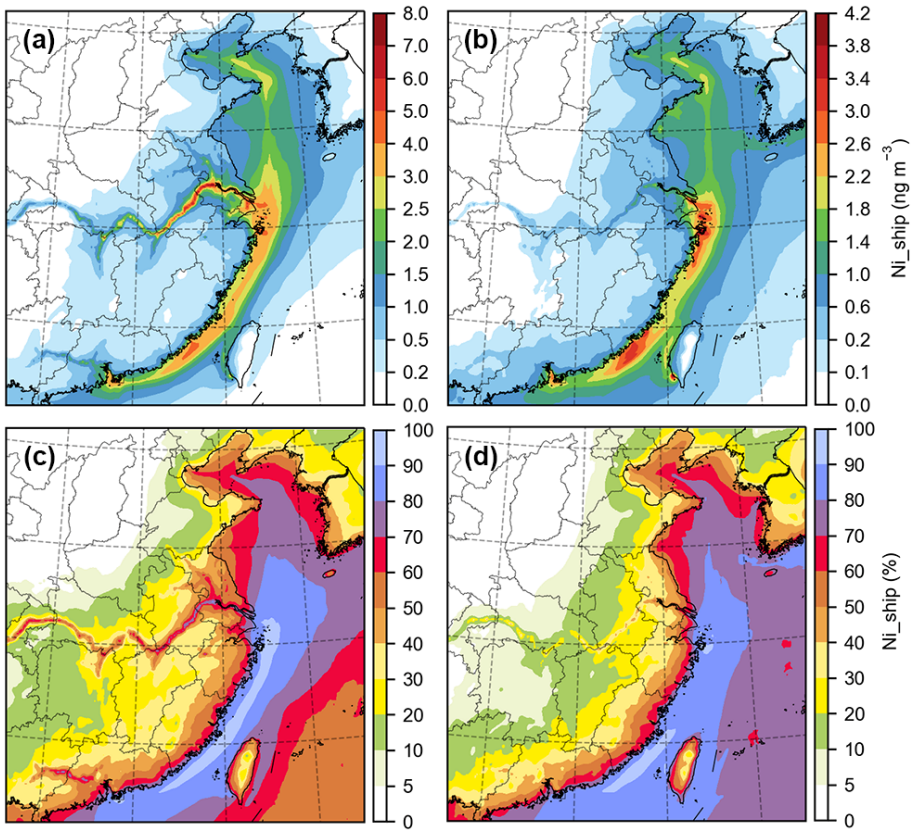

Figure S10. Impacts of ship emissions on Ni (Ni_ship): for concentration (in ng m^{-3}) in $PM_{2.5}$ in (a) 2017 and (b) 2021; and for contribution (in %) in (c) 2017 and (d) 2021.

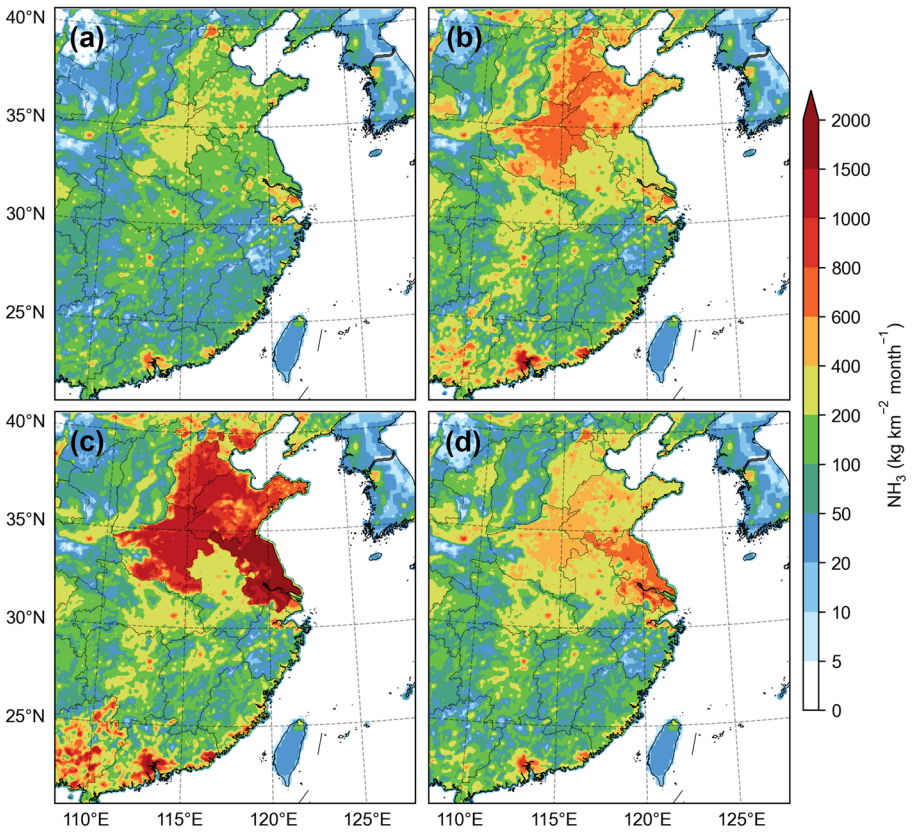

Figure S11. Spatial distributions of the NH_3 emissions for the base runs in (a) January, (b) April, (c) July, and (d) October of 2017.

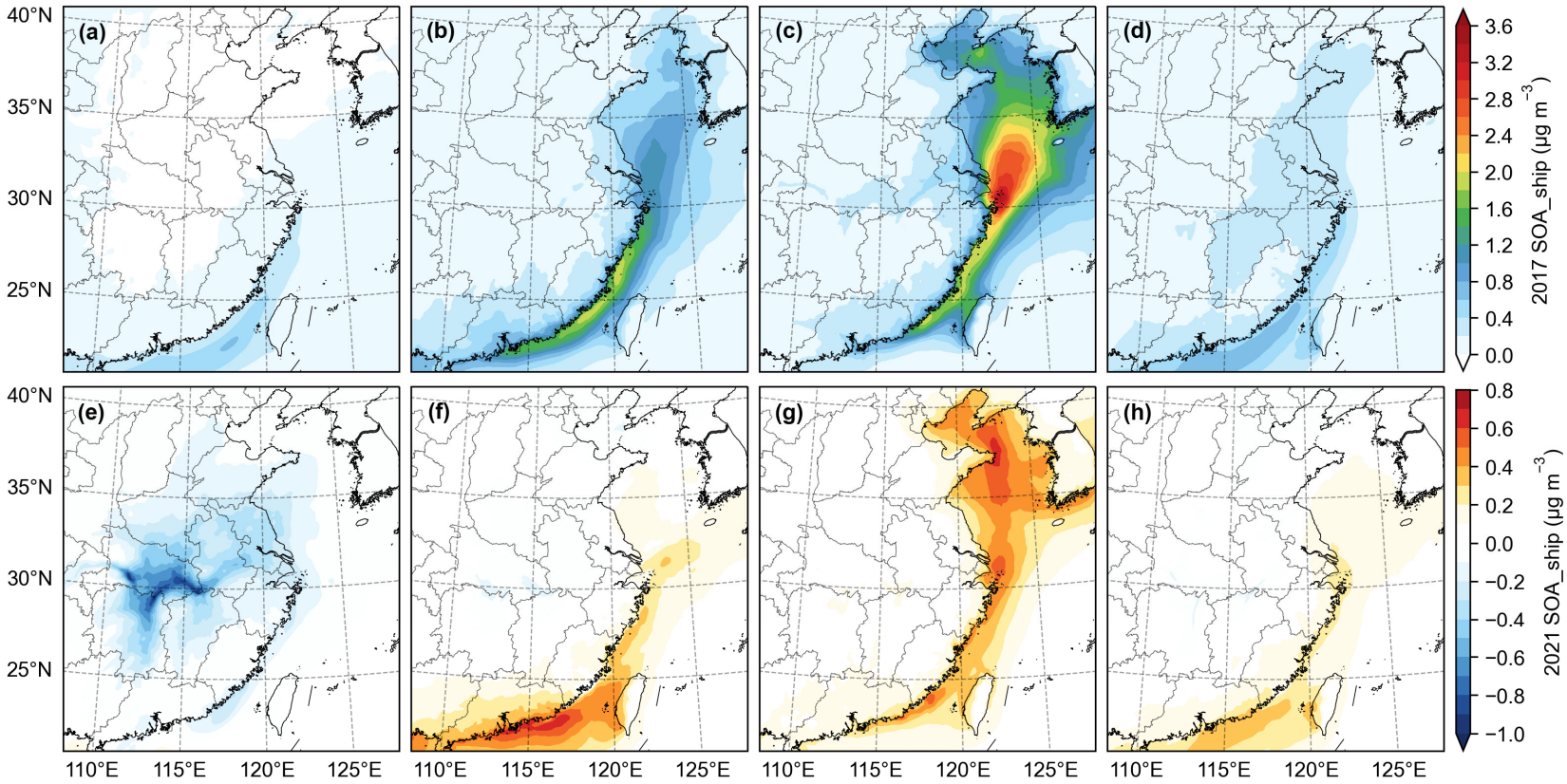

Figure S12. Seasonal variations of the potential impacts of ship emissions on secondary organic aerosols (SOA_ship) in (a) January 2017, (b) April 2017, (c) July 2017, (d) October 2017, (e) January 2021, (f) April 2021, (g) July 2021, and (h) October 2021.

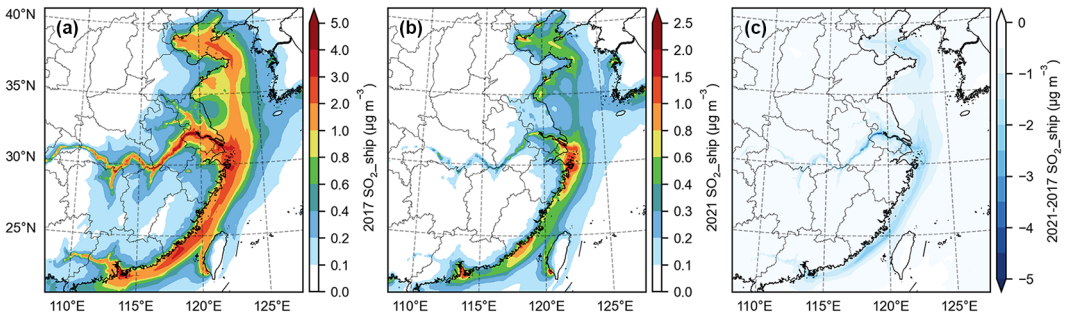

Figure S13. Impacts of ship emissions on the SO_2 concentrations (SO_2_ship) in (a) 2017 and (b) 2021, as well as its (c) absolute change from 2017 to 2021. The annual average equals the average of January, April, July, and October here and hereafter.

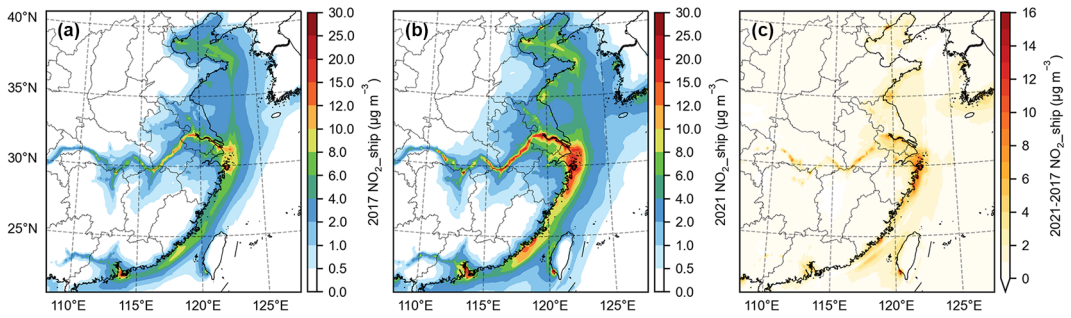

Figure S14. Impacts of ship emissions on the NO_2 concentrations (NO_2_ship) in (a) 2017 and (b) 2021, as well as its (c) absolute change from 2017 to 2021.

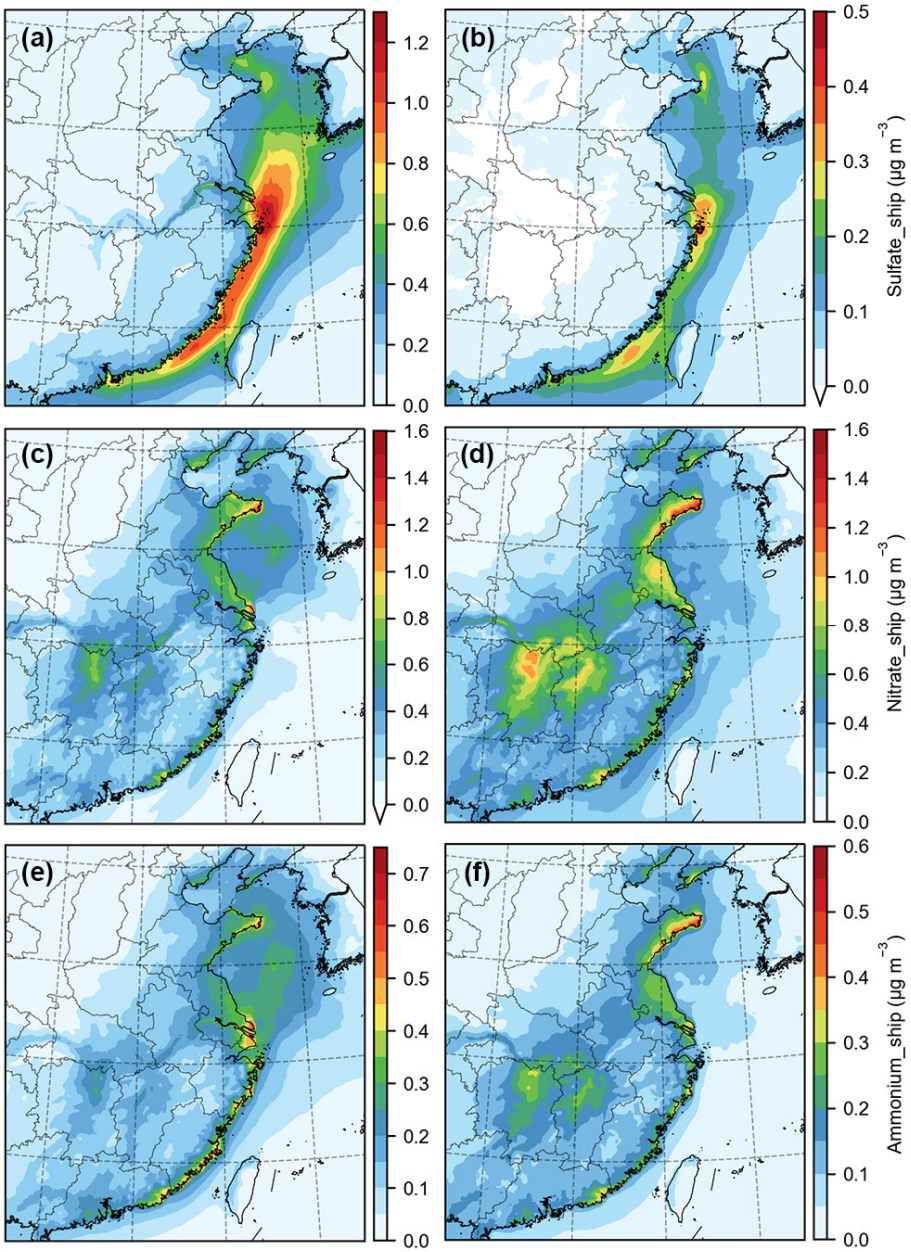

Figure S15. Potential impacts of ship emissions on sulfate (Sulfate_ship), nitrate (Nitrate_ship), and ammonium (Ammonium_ship): for sulfate in (a) 2017 and (b) 2021; for nitrate in (c) 2017 and (d) 2021; and for ammonium in (e) 2017 and (f) 2021.

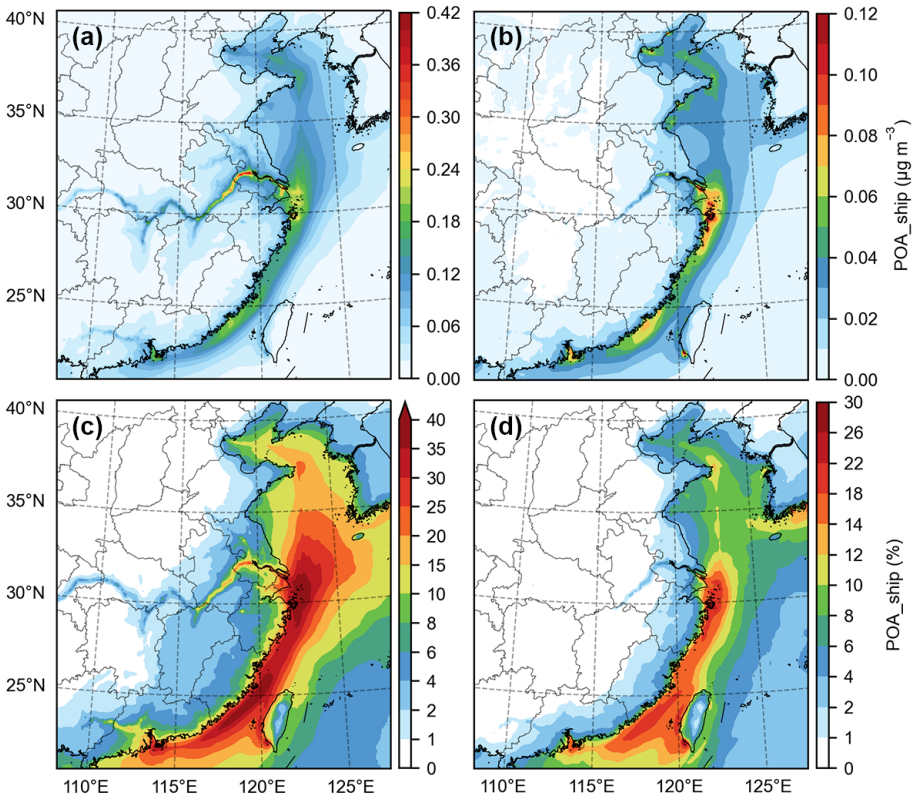

Figure S16. Impacts of ship emissions on primary organic aerosols (POA_ship): for concentration (in μg m^{-3}) in (a) 2017 and (b) 2021; and for contribution (in %) in (c) 2017 and (d) 2021.

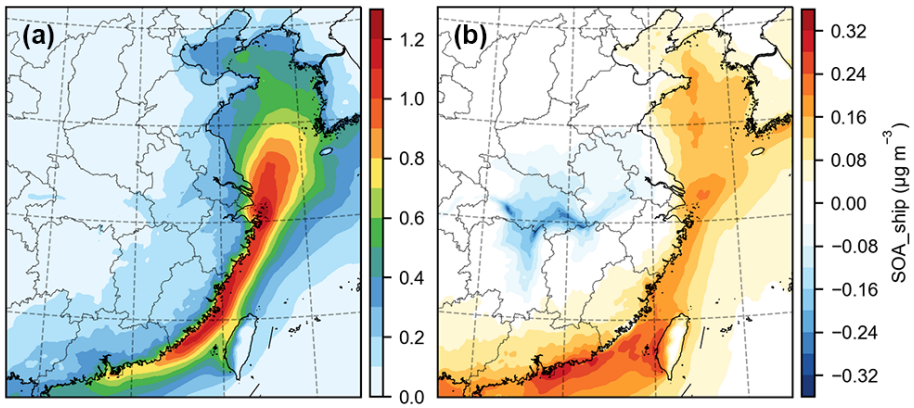

Figure S17. Potential impacts of ship emissions on secondary organic aerosols (SOA_ship) in (a) 2017 and (b) 2021.

Table S1. Summary of the staged fuel sulfur content regulations for shipping in China.

<table>
<tr><td rowspan="3">Ship type</td><td colspan="3">Emission control areas</td><td colspan="2">Outside emission control areas</td></tr>
<tr><td colspan="2">Coastal Emission Control Areas</td><td rowspan="2">Inland-River Emission Control Areas</td><td rowspan="2">Coastal waters</td><td rowspan="2">Inland-river waters</td></tr>
<tr><td>Hainan waters</td><td>Other waters</td></tr>
<tr><td>Sea-going</td><td>From 1/1/2012: ⩽3.50%
From 1/1/2019: ⩽0.50%
From 1/1/2022: ⩽0.10%</td><td>From 1/1/2012: ⩽3.50%
From 1/1/2017: ⩽0.50% in 11 core port areas (DECA 1.0)
From 1/1/2019: ⩽0.50% (DECA 2.0)</td><td>From 1/1/2019: ⩽0.50%
From 1/1/2020: ⩽0.10%</td><td colspan="2">From 1/1/2012: ⩽3.50%
From 1/1/2020: ⩽0.50%</td></tr>
<tr><td>Inland</td><td colspan="2">-</td><td rowspan="2">From 1/1/2019: ⩽10 ppm</td><td>-</td><td rowspan="2">From 1/1/2019: ⩽10 ppm</td></tr>
<tr><td>River-seas</td><td colspan="2">From 1/1/2019: ⩽0.50%</td><td>From 1/1/2012: ⩽3.50%
From 1/1/2020: ⩽0.50%</td></tr>
</table>

Note: The coastal emission control areas (CECAs) cover the marine waters within 12 nm beyond the territorial baselines. The Inland-River Emission Control Areas include the waters of the Yangtze River and the Xijiang River.

Table S2. Power-based emissions factors of main engine (ME) and auxiliary engine (AE) (unit: g kWh^{-1}).

For all areas in 2017–2018 and seas outside the CECA in 2019										
Engine type	Fuel type	SO_2	NO_x	CO	NMVOCs	PM_{10}	$PM_{2.5}$	NH_3	V	Ni
ME_SSD	HSFO	10.30	14.4	0.54	0.632	1.39	1.2788	4.90×10^{-3}	3.18×10^{-2}	1.03×10^{-2}
ME_MSD	HSFO	11.31	10.5	0.54	0.527	1.39	1.2788	2.90×10^{-3}	1.03×10^{-2}	3.51×10^{-3}
ME_HSD	MDO/MGO	0.42	7.7	0.54	0.527	0.18	0.1656	2.30×10^{-4}	4.25×10^{-5}	7.77×10^{-5}
AE	LSFO	2.12	11.2	0.54	0.421	0.73	0.6716	8.60×10^{-6}	5.42×10^{-4}	1.03×10^{-3}
For the CECA in 2019										
Engine type	Fuel type	SO_2	NO_x	CO	NMVOCs	PM_{10}	$PM_{2.5}$	NH_3	V	Ni
ME_SSD	LSHFO	1.91	14.4	0.54	0.632	0.73	0.6716	4.90×10^{-3}	1.26×10^{-2}	1.03×10^{-2}
ME_MSD	LSHFO	2.09	10.5	0.54	0.527	0.73	0.6716	2.90×10^{-3}	4.10×10^{-3}	3.51×10^{-3}
ME_HSD	MDO/MGO	0.42	7.7	0.54	0.527	0.18	0.1656	2.30×10^{-4}	4.25×10^{-5}	7.77×10^{-5}
AE	ULSFO/ LSFO	1.25	11.2	0.54	0.421	0.46	0.4232	8.60×10^{-6}	2.15×10^{-4}	6.16×10^{-4}
For sea areas in 2020–2021										
Engine type	Fuel type	SO_2	NO_x	CO	NMVOCs	PM_{10}	$PM_{2.5}$	NH_3	V	Ni
ME_SSD	LSHFO	1.91	14.4	0.54	0.632	0.73	0.6716	4.90×10^{-3}	3.18×10^{-3}	6.16×10^{-3}
ME_MSD	LSHFO	2.09	10.5	0.54	0.527	0.73	0.6716	2.90×10^{-3}	1.03×10^{-3}	2.10×10^{-3}
ME_HSD	MDO/MGO	0.42	7.7	0.54	0.527	0.18	0.1656	2.30×10^{-4}	4.25×10^{-5}	7.77×10^{-5}
AE	ULSFO/ LSFO	1.25	11.2	0.54	0.421	0.46	0.4232	8.60×10^{-6}	9.63×10^{-5}	5.54×10^{-4}

Note: ME and AE are main engine and auxiliary engine, respectively. SSD, MSD, and HSD are slow-speed diesel, medium-speed diesel, and high-speed diesel, respectively. HSFO is high sulfur fuel oil with a sulfur content of ~2.7%. LSFO is low sulfur fuel oil with a sulfur content of ~0.5%. ULSFO is ultra-low sulfur fuel oil with a sulfur content of less than 0.1%. The sulfur content of marine diesel oil (MDO) and marine gas oil (MGO) is assumed to be ~0.1%.

Table S3. Source of emission factors of V and Ni from different sectors.

Power-based emission factors of V and Ni from shipping					
Engine type	Fuel type	Fuel sulfur content (%)	V (g kWh^{-1})	Ni (g kWh^{-1})	Reference
ME_SSD	HFO	2.85	1.99×10^{-2}	8.69×10^{-3}	Agrawal et al. (2008a)
		2.05	5.60×10^{-2}	1.27×10^{-2}	Agrawal et al. (2008b)
		2.70	1.94×10^{-2}	0.95×10^{-2}	Celo et al. (2015)
ME_MSD	HFO	2.70	1.43×10^{-2}	4.10×10^{-3}	Sippula et al. (2014)
		1.48	6.80×10^{-3}	2.43×10^{-3}	Celo et al. (2015)
		2.21	1.23×10^{-2}	0.55×10^{-2}	
		1.60	7.90×10^{-3}	2.00×10^{-3}	Streibel et al. (2017)
ME_HSD	MDO	0.08	4.25×10^{-5}	7.77×10^{-5}	Zhang et al. (2016)
AE_MSD	RME180 (LSFO)	0.412–0.501	1.89×10^{-4}	1.03×10^{-3}	Hou et al. (2023)
	MGO	0.0172–0.0461	3.52×10^{-6}	7.63×10^{-5}	
Mass fractions of V and Ni in $PM_{2.5}$ from other sources					
Sector		V (%)		Ni (%)	Reference
Industry		0.012		0.0265	Liu et al. (2018)
Power		0.019		0.050	
Residential		0.002		0.005	
Transportation		0.006		0.014	

Table S4. Mapping of $PM_{2.5}$ components to the AERO7 species.

Species	Industry	Power	Residential	Land-based transportation	Shipping (HSFO)	Shipping (LSHFO)
PAL	4.71×10^{-2}	5.26×10^{-2}	6.70×10^{-3}	3.45×10^{-2}	9.30×10^{-5}	2.17×10^{-2}
PCA	3.27×10^{-2}	2.56×10^{-2}	1.16×10^{-2}	1.04×10^{-2}	3.29×10^{-2}	3.29×10^{-2}
PCL	1.04×10^{-2}	1.48×10^{-2}	9.05×10^{-4}	6.90×10^{-3}	5.47×10^{-3}	9.25×10^{-4}
PEC	5.49×10^{-2}	3.16×10^{-2}	2.40×10^{-1}	1.01×10^{-1}	4.09×10^{-2}	6.98×10^{-2}
PFE	2.14×10^{-2}	3.34×10^{-2}	8.59×10^{-3}	1.89×10^{-2}	4.98×10^{-3}	6.71×10^{-3}
PK	3.60×10^{-3}	4.90×10^{-3}	5.33×10^{-3}	2.40×10^{-3}	8.38×10^{-4}	8.38×10^{-4}
PMG	1.11×10^{-2}	1.38×10^{-2}	2.90×10^{-3}	1.63×10^{-2}	8.71×10^{-4}	8.71×10^{-4}
PMN	8.40×10^{-4}	4.50×10^{-4}	1.50×10^{-4}	1.90×10^{-4}	5.03×10^{-4}	5.03×10^{-4}
PNA	3.00×10^{-3}	3.60×10^{-3}	2.02×10^{-4}	3.20×10^{-3}	6.19×10^{-3}	6.19×10^{-3}
PNCOM	4.40×10^{-2}	4.23×10^{-2}	1.79×10^{-1}	6.33×10^{-2}	1.42×10^{-1}	8.16×10^{-2}
PNH4	3.36×10^{-2}	2.69×10^{-2}	1.41×10^{-2}	7.90×10^{-3}	2.26×10^{-2}	2.29×10^{-2}
PNO3	2.26×10^{-2}	2.19×10^{-2}	3.15×10^{-3}	1.41×10^{-2}	1.27×10^{-2}	3.23×10^{-3}
POC	1.10×10^{-1}	1.06×10^{-1}	4.48×10^{-1}	2.53×10^{-1}	5.66×10^{-1}	3.26×10^{-1}
PSI	5.51×10^{-2}	5.94×10^{-2}	6.86×10^{-3}	3.45×10^{-2}	6.31×10^{-3}	5.03×10^{-2}
PSO4	1.93×10^{-1}	1.71×10^{-1}	3.32×10^{-2}	5.12×10^{-2}	1.17×10^{-1}	5.77×10^{-2}
PTI	2.20×10^{-3}	4.50×10^{-3}	4.00×10^{-4}	4.50×10^{-3}	1.89×10^{-5}	1.89×10^{-5}

Note: The profiles of industry, power, residential, and transportation sectors for $PM_{2.5}$ excluding V and Ni are obtained from Liu et al. (2017). The mass fractions before the IMO Regulation (2017−2019) and after 2020 were referenced from Huang et al. (2018a) and Yang et al. (2022), respectively.

Table S5. Convert factors of NMVOCs emissions from shipping to lumped species in the CB6 mechanism.

Species	Convert factor (mol kg^{-1})	Mass fraction
ACET	2.12	12.3%
ALD2	0.43	1.9%
ALDX	1.47	5.5%
BENZ	0.30	2.3%
ETH	0.57	1.6%
ETHA	0.14	0.4%
ETHY	0.47	1.2%
ETOH	0	0
FORM	0	0
IOLE	0.23	1.3%
ISOP	0.04	0.3%
KET	0.31	0.6%
MEOH	0	0
NAPH	0.25	3.2%
OLE	1.80	5.7%
PAR	20.83	30.2%
PRPA	0.15	0.7%
SOAALK	2.25 (0.108PAR)	-
TERP	0	0
TOL	1.83	16.9%
XYLMN	1.49	15.8%

Note: The convert factors were based on the median VOC profiles from the literature (Agrawal et al., 2008a; Huang et al., 2018b; Zhang et al., 2024b).

Table S6. Vertical layer allocation of emission sectors for CMAQ input.

Layer	Height (m)	Shipping (marine)	Shipping (inland)	Land-based transportation	NH_3
1	0–50	20%	100%	100%	90%
2	50–109	80%	0	0	2%
3	109–179	0	0	0	6%
4	179–261	0	0	0	2%
5	261–358	0	0	0	0
6	358–472	0	0	0	0
7	472–603	0	0	0	0
Layer	Industry (VOCs)	Industry (except VOCs)	Power	Residential	Biogenic
1	50%	0	0	100%	100%
2	30%	20%	10%	0	0
3	16%	60%	10%	0	0
4	4%	20%	30%	0	0
5	0	0	20%	0	0
6	0	0	20%	0	0
7	0	0	10%	0	0

Note: The PKU-NH3 inventory in 2017 is used for non-shipping NH_3 in mainland China instead of the MEIC inventory.

Table S7. Detailed information on the studied cities and the monitoring sites.

Region	City	Port type	Latitude (cell center)	Longitude (cell center)	Meteorological station ID	Air quality monitoring station ID	Air quality data size
Bohai Bay	Dalian	Sea	38.923	121.601	54662	1109A, 1110A, 1011A, 1012A, 1013A	8038
	Yingkou	Sea	37.466	121.429	54471	1596A, 1597A, 1598A, 1599A	8057
	Caofeidian	Sea	39.229	118.403	54535	3457A	1817**
	Tianjin (downtown)*	Inland	39.141	117.185	54527	1015A, 1017A, 1018A, 1019A, 1021A, 2860A, 2922A	8032
	Tianjin (Binhai)	Estuary	39.057	117.739	54623	1023A	8030
	Yantai	Sea	40.619	122.243	54765	1643A, 1645A	8016
Yellow Sea	Qingdao	Sea	36.111	120.413	54857	1309A, 1310A, 1311A, 1312A, 1313A	8028
	Rizhao	Sea	35.437	119.442	54945	1659A, 1660A, 1661A, 3507A	8023
	Lianyungang	Sea	34.664	119.219	58040	1173A, 3434A, 3664A	7973
Yangtze River Delta	Shanghai	Estuary/ Sea/ Inland	31.217	121.437	58370	1141A, 1142A, 1143A, 1144A, 1145A, 1147A, 1148A, 1149A, 1150A, 3265A, 3268A, 3270A, 3271A, 3273A	8061
	Ningbo	Sea	29.877	121.634	58562	1234A, 1235A, 1236A, 1237A, 1239A, 1240A, 1241A, 2871A, 3710A	8064
	Zhoushan	Sea	30.029	122.236	58477	1258A, 1259A, 1260A	8064
	Hangzhou	Inland	30.257	120.155	58457	1223A, 1224A, 1227A, 1228A, 1230A	8036
	Nantong	Inland	32.05	120.911	58259	1168A, 1169A, 1170A, 1171A, 1172A, 3432A	8058
	Zhangjiagang	Inland	31.884	120.601	58353	1993A, 1994A	8061
	Nanjing	Inland	32.039	118.776	58238	1151A, 1152A, 1153A, 1154A, 1155A, 1156A, 1158A	8037
Fujian	Fuzhou	Estuary	26.067	119.297	58847	1282A, 1283A, 1284A, 1285A	8037
	Xiamen	Sea	24.54	118.153	59130	1287A, 1288A, 2842A, 3527A	8059
Pearl River Delta	Shenzhen	Estuary	22.602	114.025	59493	1356A, 1357A, 1358A, 1359A, 3305A, 3306A	8036
	Guangzhou	Estuary/ Inland	23.083	113.313	59287	1345A, 1346A, 1348A, 1349A, 1352A, 2846A, 3302A	8037
	Zhuhai	Estuary	26.1	123.771	59487	1367A, 1368A	8017
Beibu Gulf	Qinzhou	Sea	21.935	108.581	59632	2502A, 2503A, 2504A, 3404A	8064
Yantze River/ Central region	Wuhan*	Inland	30.649	114.262	57494	1325A, 1326A, 1327A, 1328A, 1331A, 1333A	8033
Northern region	Beijing*	-	39.905	116.396	54511	1001A, 1003A, 1004A, 1005A, 1006A, 1007A, 1011A	7987

* Tianjin (downtown), Wuhan, and Beijing are not included in the 21 representative port cities studied in this paper, and the observational data are only used in the evaluation of the model performance.

Table S8. Ship emissions in the 200-nm zone and the coastal provinces of Chinese mainland and their contributions to the total anthropogenic emissions in these areas.

Shipping	SO_2 (kt)	NO_x (kt)	CO (kt)	$PM_{2.5}$ (kt)	V (t)	Ni (t)
January 2017	42.9	102.9	4.6	7.3	122.6	42.4
April 2017	59.9	142.5	6.3	10.2	172.9	59.6
July 2017	58.0	133.9	5.7	9.5	163.1	56.0
October 2017	54.8	132.0	5.9	9.6	157.6	54.6
April 2018	86.6	199.7	8.8	14.5	249.1	85.6
April 2019	47.9	222.8	10.0	10.2	150.4	62.0
April 2020	20.0	212.8	9.6	7.8	23.1	47.3
January 2021	20.7	220.0	9.9	7.9	21.5	44.7
April 2021	20.8	216.7	9.7	7.9	21.2	44.2
July 2021	17.0	179.6	7.8	6.3	17.1	35.7
October 2021	20.1	216.6	9.9	7.7	20.5	42.9
2017 average per month	53.9	127.8	5.6	9.2	154.0	53.1
2021 average per month	19.6	208.2	9.3	7.4	20.1	41.9
Contribution of shipping	SO_2 (%)	NO_x (%)	CO (%)	$PM_{2.5}$ (%)	V (%)	Ni (%)
January 2017	10.4	11.3	0.1	2.7	87.0	50.1
April 2017	15.6	14.6	0.2	4.8	90.0	57.8
July 2017	15.0	13.5	0.1	4.5	89.6	56.5
October 2017	14.7	13.5	0.2	4.6	89.6	56.7
April 2018	24.4	19.5	0.2	7.3	93.5	68.6
April 2019	16.7	21.9	0.3	5.5	90.2	62.6
April 2020	8.4	22.4	0.3	4.6	60.4	58.0
January 2021	7.3	22.3	0.2	3.5	57.0	54.6
April 2021	8.8	22.7	0.3	4.6	58.4	56.3
July 2021	7.0	18.6	0.2	3.7	52.1	50.0
October 2021	8.0	21.3	0.3	4.3	56.0	54.0
2017 average	13.9	13.2	0.1	4.0	89.2	55.5
2021 average	7.7	21.2	0.3	4.0	56.0	53.8

Note: The anthropogenic emissions from sources excluding shipping are obtained from the MEIC inventory, and their values in 2020 (the latest year of the MEIC) are used to represent those in 2021.

Table S9. Comparison of hourly meteorological elements between simulated results and observational data.

	2-m temperature				Relative humidity				10-m wind speed				10-m wind direction (°)	
City	r	NMB (%)	RMSE (℃)	IoA	r	NMB (%)	RMSE (%)	IoA	r	NMB (%)	RMSE ($m\ s^{-1}$)	IoA	$\overline{Obs}$	$\overline{Sim}$
Shanghai	0.97	-0.2	2.4	0.98	0.78	-9.0	15.5	0.86	0.51	95.5	2.9	0.56	87.7	96.5
Ningbo	0.97	0.1	2.3	0.98	0.75	-5.0	14.2	0.86	0.53	15.0	2.2	0.72	31.3	110.2
Zhoushan	0.96	-5.6	2.4	0.98	0.73	-0.7	13.2	0.85	0.43	24.4	2.4	0.64	47.8	92.7
Nantong	0.97	3.9	2.5	0.98	0.80	-16.8	18.4	0.82	0.61	10.4	2.0	0.77	74.6	81.5
Zhangjiagang	0.97	3.0	2.7	0.98	0.79	-14.1	17.0	0.84	0.51	37.8	2.3	0.67	61.3	81.0
Nanjing	0.97	3.5	2.7	0.98	0.80	-17.0	17.9	0.83	0.51	19.3	2.1	0.70	73.5	81.6
Hangzhou	0.96	2.8	2.8	0.98	0.76	-14.2	16.8	0.82	0.46	13.3	2.1	0.68	5.2	48.4
Fuzhou	0.95	-0.9	2.5	0.97	0.60	-7.1	16.0	0.76	0.41	-9.1	2.0	0.65	67.4	62.6
Xiamen	0.94	-1.1	2.3	0.97	0.69	-9.8	15.6	0.80	0.56	36.6	2.1	0.71	89.2	59.0
Guangzhou	0.91	7.5	3.4	0.93	0.68	-20.4	21.4	0.71	0.49	53.1	2.3	0.64	1.9	88.8
Shenzhen	0.91	0.3	2.5	0.95	0.75	-9.1	14.7	0.82	0.48	72.2	2.6	0.59	62.1	87.7
Zhuhai	0.90	1.2	2.6	0.94	0.74	-11.6	15.7	0.80	0.48	58.3	2.3	0.60	85.8	94.8
Qinzhou	0.88	1.8	3.1	0.93	0.72	-11.6	15.5	0.79	0.56	0.6	2.1	0.74	6.2	35.3
Tianjin (downtown)	0.97	3.9	2.9	0.98	0.78	-20.9	20.3	0.83	0.58	10.3	2.1	0.75	142.9	203.2
Tianjin (Binhai)	0.97	-2.9	2.8	0.98	0.76	-9.1	17.2	0.86	0.56	28.2	2.3	0.72	155.2	160.7
Caofeidian	0.97	-2.5	2.6	0.98	0.77	-16.8	19.1	0.84	0.60	32.6	2.3	0.73	206.3	218.3
Yingkou	0.98	-1.7	2.3	0.99	0.72	-8.2	16.6	0.84	0.58	14.4	2.6	0.75	238.0	238.8
Dalian	0.98	-2.7	2.3	0.99	0.82	2.4	14.6	0.90	0.57	16.8	2.4	0.74	312.5	282.4
Yantai	0.98	0.2	2.3	0.99	0.78	-2.0	14.7	0.88	0.58	-1.6	2.5	0.75	291.2	280.7
Qingdao	0.98	0.1	2.3	0.98	0.78	-7.9	15.6	0.87	0.58	-2.9	2.3	0.76	80.2	97.5
Rizhao	0.97	1.7	2.7	0.98	0.77	-11.2	17.4	0.86	0.54	-4.3	2.4	0.72	32.2	31.7
Lianyungang	0.96	2.3	2.8	0.98	0.74	-14.1	18.4	0.82	0.61	25.8	2.2	0.75	68.8	66.8
Wuhan	0.96	3.4	2.7	0.98	0.66	-19.8	21.7	0.72	0.56	51.1	2.2	0.68	30.0	34.8
Xi'an	0.96	10.9	3.3	0.97	0.72	-27.8	24.8	0.75	0.41	22.5	2.0	0.63	44.3	33.4
Beijing	0.97	4.9	3.2	0.98	0.77	-22.4	20.3	0.83	0.54	22.0	2.1	0.72	297.9	256.1

Note: $\overline{Obs}$ and $\overline{Sim}$ are mean values of observational data and simulated results, respectively. The hourly wind direction observational data of Guangzhou started in 2018.

Table S10. Comparison of the concentrations of the main air pollutants in the studied cities between simulated results and observational data.

	SO_2				NO_2				MDA8 O_3				$PM_{2.5}$			
City	r	NMB (%)	RMSE ($\mu g\ m^{-3}$)	IoA	r	NMB (%)	RMSE ($\mu g\ m^{-3}$)	IoA	r	NMB (%)	RMSE ($\mu g\ m^{-3}$)	IoA	r	NMB (%)	RMSE ($\mu g\ m^{-3}$)	IoA
Shanghai	0.48	79.0	10.6	0.50	0.58	63.2	34.7	0.61	0.76	-26.6	42.1	0.79	0.55	-26.6	22.5	0.71
Ningbo	0.51	-34.5	5.0	0.61	0.51	16.7	23.1	0.69	0.6	-10.7	37.6	0.76	0.54	-30.7	20.0	0.70
Zhoushan	0.51	-43.9	4.8	0.60	0.45	22.3	20.6	0.59	0.53	-10.7	32.2	0.70	0.50	-26.9	15.5	0.69
Nantong	0.51	-38.6	10.2	0.66	0.58	16.3	24.1	0.75	0.68	-15.8	36.9	0.78	0.56	-35.8	25.5	0.69
Zhangjiagang	0.29	-15.3	10.5	0.50	0.52	23.9	24.9	0.68	0.71	-16.4	38.0	0.80	0.58	-33.0	24.9	0.71
Nanjing	0.33	-12.1	8.7	0.59	0.52	22.5	28.1	0.69	0.65	-17.5	40.0	0.77	0.57	-14.5	23.8	0.75
Hangzhou	0.42	-12.1	5.8	0.61	0.45	9.5	27.0	0.65	0.74	-4.2	33.3	0.85	0.51	-32.4	25.8	0.68
Fuzhou	0.24	-34.0	3.5	0.47	0.37	-21.1	17.7	0.61	0.55	3.5	28.4	0.72	0.35	-44.3	19.6	0.57
Xiamen	0.40	-25.6	6.4	0.61	0.35	41.9	27.3	0.54	0.51	4.1	28.1	0.72	0.40	-19.5	17.6	0.63
Guangzhou	0.46	-5.9	6.0	0.63	0.37	-14.4	33.2	0.60	0.54	5.1	44.7	0.68	0.44	-43.4	25.2	0.55
Shenzhen	0.26	67.8	7.2	0.31	0.37	54.5	29.7	0.53	0.58	-5.4	34.9	0.74	0.52	-33.6	15.6	0.64
Zhuhai	0.32	-16.3	4.4	0.56	0.48	-34.2	22.1	0.64	0.54	12.3	40.0	0.72	0.50	-42.8	17.5	0.62
Qinzhou	0.27	-77.6	13.8	0.39	0.28	-72.2	18.0	0.45	0.51	20.1	33.2	0.67	0.58	-48.4	26.4	0.62
Tianjin (downtown)	0.49	24.5	13.1	0.67	0.58	46.1	32.9	0.68	0.78	-38.1	52.1	0.73	0.58	-37.6	45.1	0.69
Tianjin (Binhai)	0.34	-31.7	14.3	0.50	0.50	-32.9	33.5	0.66	0.71	-10.4	32.9	0.82	0.59	-44.9	41.6	0.69
Caofeidian	0.21	-39.8	7.9	0.47	0.60	-14.1	18.5	0.76	0.69	-12.7	32.8	0.80	0.60	-29.2	26.6	0.73
Yingkou	0.56	-47.4	14.4	0.58	0.54	-18.4	18.3	0.72	0.64	-26.3	45.2	0.69	0.54	-42.2	38.7	0.64
Dalian	0.42	-16.3	10.9	0.59	0.4	51.1	27.2	0.54	0.58	-33.8	46.3	0.61	0.53	-13.6	25.1	0.72
Yantai	0.39	-47.1	13.9	0.50	0.52	-18.1	19.5	0.70	0.52	-20.0	38.4	0.66	0.60	-18.6	23.2	0.76
Qingdao	0.60	9.5	9.7	0.76	0.55	28.2	23.8	0.70	0.52	-28.4	44.8	0.63	0.56	-8.0	28.8	0.73
Rizhao	0.56	-32.0	8.4	0.69	0.53	-26.9	22.5	0.68	0.62	-13.4	32.1	0.75	0.62	-30.9	33.4	0.74
Lianyungang	0.54	-65.5	14.8	0.51	0.52	-29.1	19.5	0.68	0.57	-13.3	34.2	0.72	0.59	-32.7	30.1	0.74
Wuhan	0.44	187.8	31.4	0.23	0.53	5.4	27.4	0.72	0.67	0.5	29.2	0.81	0.65	6.5	31.8	0.77
Xi'an	0.68	-9.5	11.2	0.75	0.36	-34.0	34.1	0.59	0.77	-3.2	34.0	0.84	0.62	-46.7	60.9	0.58
Beijing	0.48	69.1	11.5	0.62	0.53	66.2	45.1	0.59	0.76	-28.8	44.5	0.79	0.58	-30.2	49.7	0.70

Note: The concentrations of SO_2, NO_2, and $PM_{2.5}$ are in hourly resolution. The daily maximum 8-h average (MDA8) O_3 concentrations are in daily resolution. The observational data from Caofeidian started from 17 April 2021.

Table S11. Comparison of the hourly concentrations of sulfate, nitrate, and ammonium between simulated results and observational data at the Pudong site of Shanghai.

SNA	Parameter	Jan. 2017	Apr. 2017	Jul. 2017	Oct. 2017	Apr. 2018	Apr. 2019	Apr. 2020	Jan. 2021	Apr. 2021	Jul. 2021	Oct. 2021
SO_4^{2-}	N (obs)	707	702	691	693	693	557	673	691	707	738	706
	N (sim)	744	720	744	744	720	720	720	744	720	744	744
	$\overline{Obs}$ (μg m^{-3})	9.47	8.06	5.96	4.83	6.82	6.21	4.33	5.13	4.71	3.41	3.37
	$\overline{Sim}$ (μg m^{-3})	6.62	7.02	5.12	3.87	4.99	6.02	4.01	5.00	4.21	2.71	3.13
	r	0.41	0.10	0.71	0.30	0.33	0.04	0.03	0.19	0.32	0.34	0.25
	NMB (%)	-30.4	-12.1	-15.4	-19.3	-25.7	-1.8	-6.9	-3.0	-10.1	-20.2	-6.2
	RMSE (μg m^{-3})	7.33	6.48	2.73	3.94	4.34	6.41	3.22	3.61	4.92	2.27	2.60
	IoA	0.60	0.43	0.83	0.45	0.54	0.32	0.34	0.50	0.51	0.58	0.49
NO_3^-	N (obs)	707	702	691	691	693	557	673	691	707	738	706
	N (sim)	744	720	744	744	720	720	720	744	720	744	744
	$\overline{Obs}$ (μg m^{-3})	11.42	10.45	2.58	4.11	8.73	11.62	8.30	9.08	8.59	2.46	3.59
	$\overline{Sim}$ (μg m^{-3})	14.56	5.48	1.71	1.94	5.26	9.27	5.88	14.38	5.17	1.30	3.05
	r	0.61	0.36	0.54	0.33	0.38	0.46	0.27	0.26	0.52	0.34	0.65
	NMB (%)	26.0	-47.4	-33.3	-51.1	-41.2	-16.0	-29.0	63.8	-39.0	-46.8	-7.8
	RMSE (μg m^{-3})	11.00	9.28	4.45	5.61	9.02	11.00	7.48	12.42	8.88	5.01	5.67
	IoA	0.75	0.47	0.61	0.54	0.55	0.69	0.55	0.46	0.67	0.54	0.89
NH_4^+	N (obs)	707	702	675	686	692	556	673	691	707	730	706
	N (sim)	744	720	744	744	720	720	720	744	720	744	744
	$\overline{Obs}$ (μg m^{-3})	7.48	5.91	3.15	2.63	4.70	5.49	3.93	5.50	4.16	1.88	1.99
	$\overline{Sim}$ (μg m^{-3})	6.20	6.35	2.00	1.51	2.77	4.53	2.60	5.45	2.44	0.90	1.51
	r	0.65	0.47	0.67	0.35	0.38	0.43	0.22	0.20	0.52	0.43	0.77
	NMB (%)	-17.9	9.1	-36.6	-41.2	-41.6	-14.5	-33.0	0.9	-40.6	-51.5	-23.1
	RMSE (μg m^{-3})	4.86	6.02	2.21	2.97	3.99	4.42	3.24	4.07	3.95	2.06	1.66
	IoA	0.78	0.63	0.76	0.48	0.53	0.66	0.53	0.54	0.68	0.63	0.86

Note: $\overline{Obs}$ and $\overline{Sim}$ are mean values of observational data and simulated results, respectively. N(obs) and N (sim) are numbers of observational data and simulated results, respectively.

Table S12. Comparison of hourly V and Ni concentrations between simulated results and observational data at the Pudong site of Shanghai during the simulation period.

Metal	Parameter	Jan. 2017	Apr. 2017	Jul. 2017	Oct. 2017	Apr. 2018	Apr. 2019	Apr. 2020	Jan. 2021	Apr. 2021	Jul. 2021	Oct. 2021
V	N (obs)	679	623	596	733	567	503	281	233	374	394	361
	N (sim)	744	720	744	744	720	720	720	744	720	744	744
	$\overline{Obs}$ (ng m^{-3})	10.76	17.02	9.70	8.27	16.32	7.23	1.23	1.49	1.41	1.46	1.11
	$\overline{Sim}$ (ng m^{-3})	15.18	17.65	11.08	9.93	15.81	7.73	2.21	2.41	1.86	0.90	1.43
	r	0.43	0.12	0.61	0.29	0.33	0.56	0.41	0.35	0.24	0.25	0.13
	NMB (%)	46.2	10.0	27.4	20.8	0.9	15.9	110.0	87.9	45.5	-37.1	55.4
	RMSE (ng m^{-3})	14.22	22.40	10.00	12.49	16.83	7.22	2.14	2.21	1.73	1.23	1.47
	IoA	0.63	0.41	0.75	0.48	0.51	0.73	0.54	0.53	0.47	0.48	0.41
Ni	N (obs)	741	714	714	735	612	608	703	743	701	621	738
	N (sim)	744	720	744	744	720	720	720	744	720	744	744
	$\overline{Obs}$ (ng m^{-3})	5.08	7.21	4.60	4.45	7.64	5.39	3.59	3.72	3.88	2.92	3.47
	$\overline{Sim}$ (ng m^{-3})	6.83	7.02	4.56	3.91	6.01	4.22	4.14	4.84	3.37	1.81	2.90
	r	0.33	0.17	0.59	0.21	0.30	0.45	0.28	0.27	0.31	0.26	0.42
	NMB (%)	35.0	-2.2	0.5	-11.8	-22.0	-22.5	16.5	30.2	-13.4	-43.3	-17.1
	RMSE (ng m^{-3})	5.46	7.53	3.42	5.04	6.70	5.02	3.54	4.12	3.06	2.36	2.62
	IoA	0.56	0.44	0.76	0.44	0.46	0.58	0.50	0.49	0.58	0.48	0.65
Ni/V	$\overline{Obs}$	0.47	0.42	0.47	0.54	0.47	0.75	2.92	2.50	2.74	2.00	3.14
	$\overline{Sim}$	0.45	0.40	0.41	0.39	0.38	0.55	1.87	2.01	1.82	2.01	2.03

Note: $\overline{Obs}$ and $\overline{Sim}$ are mean values of observational data and simulated results, respectively. N(obs) and N (sim) are numbers of observational data and simulated results, respectively.

Table S13. Comparison of the observed and simulated V and Ni concentrations in the model domain (unit: ng m^{-3}).

City	Observation			Simulation (this study)			Reference
	DECA 1.0	DECA 2.0	IMO 2020	DECA 1.0	DECA 2.0**	IMO 2020	
Shanghai	V: 11.31 Ni: 5.32	V: 7.23 Ni: 5.39	V: 1.36 Ni: 3.52	V: 13.4 Ni: 5.6	V: 7.7 Ni: 4.2	V: 1.7 Ni: 3.2	This study
Qingdao	V*: 4.01 Ni*: 3.03	V*: 1.50 Ni*: 2.13	V*: 0.84 Ni*: 3.55	V: 5.9 Ni: 4.0	V: 6.9 Ni: 3.8	V: 1.6 Ni: 3.1	Du et al. (2024)
Jiaxing	V: 5.52 Ni: 4.68	V: 4.29 Ni: 4.44	V: 1.34 Ni: 4.18	V: 8.3 Ni: 3.9	V: 5.4 Ni: 3.2	V: 1.2 Ni: 2.2	Zhang et al. (2024a)
Xiamen	V: 7.35 Ni: 3.22		V: 1.60 Ni: 1.87	V: 9.0 Ni: 3.7		V: 1.2 Ni: 2.3	Li et al. (2025)
Guangzhou	V: 1.1 Ni: 3.1					V: 1.3 Ni: 2.6	Zhang et al. (2024c)
Seoul	V: 4.6 Ni: 1.7	V: 2.1 Ni: 0.8	V: 0.4 Ni: 0.5	V: 2.3 Ni: 1.5	V: 3.2 Ni: 1.7	V: 0.6 Ni: 1.7	Yeo et al. (2024)

Note: * The observed V and Ni concentrations in Qingdao are PM_1-bound. The other data are $PM_{2.5}$-bound.

** The simulated month for the DECA 2.0 is April 2019 with peak concentrations in a year.

Table S14. Low load adjustment multipliers (LLAMs) for main engine emission factors.

Load	SO_2	NO_x	CO	NMVOCs	PM
0.01	1	11.47	19.32	59.28	19.17
0.02	1	4.63	9.68	21.18	7.29
0.03	1	2.92	6.46	11.68	4.33
0.04	1	2.21	4.86	7.71	3.09
0.05	1	1.83	3.89	5.61	2.44
0.06	1	1.6	3.25	4.35	2.04
0.07	1	1.45	2.79	3.52	1.79
0.08	1	1.35	2.45	2.95	1.61
0.09	1	1.27	2.18	2.52	1.48
0.1	1	1.22	1.96	2.2	1.38
0.11	1	1.17	1.79	1.96	1.3
0.12	1	1.14	1.64	1.76	1.24
0.13	1	1.11	1.52	1.6	1.19
0.14	1	1.08	1.41	1.47	1.15
0.15	1	1.06	1.32	1.36	1.11
0.16	1	1.05	1.24	1.26	1.08
0.17	1	1.03	1.17	1.18	1.06
0.18	1	1.02	1.11	1.11	1.04
0.19	1	1.01	1.05	1.05	1.02
0.2	1	1	1	1	1

Note: The values for PM apply to PM_{10}, $PM_{2.5}$, and all calculated chemical species including OC, EC, V, and Ni.

References

Agrawal, H., Welch, W. A., Miller, J. W., and Cocker, D. R.: Emission Measurements from a Crude Oil Tanker at Sea, Environmental Science & Technology, 42, 7098−7103, https://doi.org/10.1021/es703102y, 2008a.

Agrawal, H., Malloy, Q. G. J., Welch, W. A., Wayne Miller, J., and Cocker, D. R.: In-use gaseous and particulate matter emissions from a modern ocean going container vessel, Atmospheric Environment, 42, 5504−5510, https://doi.org/10.1016/j.atmosenv.2008.02.053, 2008b.

Celo, V., Dabek-Zlotorzynska, E., and McCurdy, M.: Chemical characterization of exhaust emissions from selected canadian marine vessels: the case of trace metals and lanthanoids, Environmental Science & Technology, 49, 5220−5226, https://doi.org/10.1021/acs.est.5b00127, 2015.

Du, J., Liu, Z., Tao, W., Wang, T., Zhao, J., Gong, W., Li, Y., Xue, L., Yang, J., Wang, C., Zhang, H., Wang, F., Sun, Y., and Zhang, Y.: Characteristics of Trace Metal Elements in Ambient Sub-Micron Particulate Matter in a Coastal Megacity of Northern China Influenced by Shipping Emissions from 2018 to 2022, Atmosphere, 15, 264, https://doi.org/10.3390/atmos15030264, 2024.

Hou, W., Liu, Z., Yu, G., Bie, S., Zhang, Y., Chen, Y., Ma, D., Zhang, F., Lou, C., Hu, X., Gui, Y., and Zhou, W.: On-board measurements of OC/EC ratio, mixing state, and light absorption of ship-emitted particles, Science of the Total Environment, 904, 166692, https://doi.org/10.1016/j.scitotenv.2023.166692, 2023.

Huang, C., Hu, Q., Wang, H., Qiao, L., Jing, S., Wang, H., Zhou, M., Zhu, S., Ma, Y., Lou, S., Li, L., Tao, S., Li, Y., and Lou, D.: Emission factors of particulate and gaseous compounds from a large cargo vessel operated under real-world conditions, Environmental Pollution, 242, 667−674, https://doi.org/10.1016/j.envpol.2018.07.036, 2018a.

Huang, C., Hu, Q., Li, Y., Tian, J., Ma, Y., Zhao, Y., Feng, J., An, J., Qiao, L., Wang, H., Jing, S., Huang, D., Lou, S., Zhou, M., Zhu, S., Tao, S., and Li, L.: Intermediate Volatility Organic Compound Emissions from a Large Cargo Vessel Operated under Real-World Conditions, Environmental Science & Technology, 52, 12934−12942, https://doi.org/10.1021/acs.est.8b04418, 2018b.

Li, J. M., Zhao, S. M., Miao, Q. Y., Wu, S. P., Zhang, J., and Schwab, J. J.: Changes in source contributions to the oxidative potential of $PM_{2.5}$ in urban Xiamen, China, Journal of Environmental Sciences, 149, 342−357, https://doi.org/10.1016/j.jes.2024.02.003, 2025.

Liu, Y., Xing, J., Wang, S., Fu, X., and Zheng, H.: Source-specific speciation profiles of $PM_{2.5}$ for heavy metals and their anthropogenic emissions in China, Environmental Pollution, 239, 544−553, https://doi.org/10.1016/j.envpol.2018.04.047, 2018.

Liu, Y., Zhang, W., Bai, Z., Yang, W., Zhao, X., Han, B., and Wang, X.: China Source Profile Shared Service (CSPSS): The Chinese $PM_{2.5}$ Database for Source Profiles, Aerosol and Air Quality Research, 17, 1501−1514, https://doi.org/10.4209/aaqr.2016.10.0469, 2017.

Seinfeld, J. H. and Pandis, S. N.: Atmospheric chemistry and physics: from air pollution to climate change, 3rd Edition, John Wiley & Sons, New York, U.S., ISBN 978-1-118-94740-1, 2016.

Sippula, O., Stengel, B., Sklorz, M., Streibel, T., Rabe, R., Orasche, J., Lintelmann, J., Michalke, B., Abbaszade, G., Radischat, C., Groger, T., Schnelle-Kreis, J., Harndorf, H., and Zimmermann, R.: Particle emissions from a marine engine: chemical composition and aromatic emission profiles under various operating conditions, Environmental Science & Technology, 48, 11721−11729, https://doi.org/10.1021/es502484z, 2014.

Streibel, T., Schnelle-Kreis, J., Czech, H., Harndorf, H., Jakobi, G., Jokiniemi, J., Karg, E., Lintelmann, J., Matuschek, G., Michalke, B., Muller, L., Orasche, J., Passig, J., Radischat, C., Rabe, R., Reda, A.,

Ruger, C., Schwemer, T., Sippula, O., Stengel, B., Sklorz, M., Torvela, T., Weggler, B., and Zimmermann, R.: Aerosol emissions of a ship diesel engine operated with diesel fuel or heavy fuel oil, Environmental Science and Pollution Research, 24, 10976−10991, https://doi.org/10.1007/s11356-016-6724-z, 2017.

Yang, L., Zhang, Q., Zhang, Y., Lv, Z., Wu, L., and Mao, H.: Real-world emission characteristics of an ocean-going vessel through long sailing measurement, Science of the Total Environment, 810, 152276, https://doi.org/10.1016/j.scitotenv.2021.152276, 2022.

Yeo, M. J., Lee, D., Na, S., Lee, D., Kim, Y. P., Park, J., and Koo, J.-H.: Variation of the concentrations of the particulate chemical components in Seoul response to the changes of major emission sources in the region: emphasis on ambient heavy metals, Journal of Atmospheric Chemistry, 82, 7, https://doi.org/10.1007/s10874-025-09473-6, 2025.

Zhang, F., Chen, Y., Tian, C., Lou, D., Li, J., Zhang, G., and Matthias, V.: Emission factors for gaseous and particulate pollutants from offshore diesel engine vessels in China, Atmospheric Chemistry and Physics, 16, 6319−-6334, https://doi.org/10.5194/acp-16-6319-2016, 2016.

Zhang, F., Shen, Y., Xu, B., Shen, J., Jin, L., Yao, L., Kuang, B., Xu, Z., Pei, X., Tang, Q., Tian, X., and Wang, Z.: Characteristics, sources, and health risks of $PM_{2.5}$-bound trace metals in northern Zhejiang Province: The effects of meteorological variables based on machine learning, Journal of Cleaner Production, 451, 142089, https://doi.org/10.1016/j.jclepro.2024.142089, 2024a.

Zhang, F., Xiao, B., Liu, Z., Zhang, Y., Tian, C., Li, R., Wu, C., Lei, Y., Zhang, S., Wan, X., Chen, Y., Han, Y., Cui, M., Huang, C., Wang, H., Chen, Y., and Wang, G.: Real-world emission characteristics of VOCs from typical cargo ships and their potential contributions to secondary organic aerosol and O_3 under low-sulfur fuel policies, Atmospheric Chemistry and Physics, 24, 8999−9017, https://doi.org/10.5194/acp-24-8999-2024, 2024b.

Zhang, Z., Tao, J., Zhang, L., Hu, B., Liu, M., Nie, F., Lu, H., Chen, L., Wu, Y., Chen, D., Wang, B., and Che, H.: Influence of sources and atmospheric processes on metal solubility in $PM_{2.5}$ in urban Guangzhou, South China, Science of the Total Environment, 951, 175807, https://doi.org/10.1016/j.scitotenv.2024.175807, 2024c.